Journal of Science: Advanced Materials and Devices 9 (2024) 100767

Contents lists available at ScienceDirect

Journal of Science: Advanced Materials and Devices

journal homepage: www.elsevier.com/locate/jsamd

Research Article

Development and characterization of novel PBI/SGO composites as possible proton exchange membranes filling the "conductivity gap"

Matteo Di Virgilio, Andrea Basso Peressut *, Sophie Provato, Saverio Latorrata

Politecnico di Milano, Department of Chemistry, Materials and Chemical Engineering "Giulio Natta", Piazza Leonardo da Vinci 32, 20133, Milano, Italy

ARTICLE INFO

Keywords:
Polybenzimidazole
Sulfonated graphene oxide
Composite membrane design
Conductivity gap
Proton conductivity
Electrochemical impedance spectroscopy

ABSTRACT

The research for non-fluorinated polymeric electrolytes able to operate at temperatures of 80–120 °C, the so-called "conductivity gap", is becoming central. Within this frame, the present work discusses the investigation of innovative self-assembling polybenzimidazole/sulfonated graphene oxide (PBI/SGO) composite membranes. A set of five samples, characterized by never-explored PBI-to-SGO mass ratios between 3:1 and 1:3, is studied through surface and cross-sectional SEM, XRD, ATR-FTIR spectroscopy, and TGA. The experimental outcomes reveal the reciprocal compatibility between PBI and SGO, whose main features appear to be evenly distributed within the composites. Water immersion tests demonstrate the excellent interplay between the membranes and the aqueous environment. EIS experiments, performed with the in-plane and through-plane configurations, disclose the improvement of the proton transfer ability (σ) in both directions. At 120 °C, PBI/SGO 1:2 achieves the highest in-plane σ of 0.113 S cm^{-1}, while PBI/SGO 1:3 shows the best through-plane σ of 0.025 S cm^{-1}. The preference toward planar proton migration is confirmed by the computation of the anisotropy factor, which is attenuated to ≈0.5 with the aid of temperature. Based on these findings, the composites with large SGO content seem to possess great potential as alternative non-fluorinated proton exchange membranes.

1. Introduction

In the next years, a comprehensive energy transition toward clean, low-carbon, and renewable alternatives will become inevitable and vital. The exacerbation of the global energy crisis, a direct consequence of the world population growth whose prospects forecasted the overcoming of 9.5 billion humans on the planet by 2050 [1], is not only fueling cost-push inflation and lowering household budgets but also aggravating the worldwide warming emergency [2]. In reaction, governments are more and more adopting short-term policy measures in compliance with the Paris Agreement and the Net Zero Emission by 2050 (NZE) scenario, seeking the mitigation of the temperature rise to 1.5 °C compared to pre-industrial levels [3]. Considering that this threshold is dramatically near, since a record of 1.4 °C was measured in October 2023 [4], the effort in finding an attainable pathway to achieve carbon neutrality, to improve energy accessibility, and to preserve environmental wellness must be maximized on a global scale.

Within this complicated scenario, proton exchange membrane fuel cells (PEMFCs) are proving to be worthy promoters of the needed revolution toward a greener world [5,6]. PEMFCs are renowned for their applicability both in stationary and portable applications, thanks to the possibility to directly generate electricity by means of the redox half-reactions taking place at the electrodes [7,8]. The solid electrolyte placed at the heart of a PEMFC can be unquestionably identified as the most important component. Nafion® by Chemours, a particular kind of perfluorinated sulfonic acid, dominated the scene for many years with more than satisfactory outcomes, thanks to its vast set of useful properties. Nevertheless, this material is affected by several issues: (i) the overall high price due to the expensive fluorination process; (ii) the impossibility to sustain temperatures higher than the typical operating ones of PEMFCs (i.e., 60–80 °C at atmospheric pressure), since it would undergo dehydration, drop in proton conductivity, and deterioration of mechanical properties [9,10]; (iii) the inclusion within the larger category of per- and polyfluoroalkyl substances (PFASs), which is strictly connected with the preservation of the environmental wellness pursued by recent policies. Indeed, PFASs are referred to as "forever chemicals", inasmuch they easily accumulate in water, air, soils, and plants. Such a strong persistency, which is dangerous for human health, depends on the

Peer review under responsibility of Vietnam National University, Hanoi.
* Corresponding author.
E-mail addresses: matteo.divirgilio@polimi.it (M. Di Virgilio), andreastefano.basso@polimi.it (A. Basso Peressut), sophie.provato@mail.polimi.it (S. Provato), saverio.latorrata@polimi.it (S. Latorrata).

https://doi.org/10.1016/j.jsamd.2024.100767
Received 15 April 2024; Received in revised form 18 July 2024; Accepted 21 July 2024
Available online 22 July 2024

strength of the carbon-fluorine covalent bond that prevents a total degradation [11,12].

The extensive research of new electrolytic membranes, especially non-fluorinated ones, able to substitute Nafion® is therefore clearly justified. Particular attention was addressed to polybenzimidazole (PBI), a linear, amorphous, thermoplastic, heterocyclic polymer with high thermal stability, remarkable chemical resistance to both acid and basic reagents, and good mechanical strength [13,14]. The shortcoming of an innate scarce proton conductivity can be solved by combining the PBI matrix with some proton conductive species and by imbibing the resulting composites in phosphoric acid (PA), which can easily bond with the N–H moieties of the imidazole rings to allow a facilitated migration of protons along the chains [15,16]. Graphene oxide (GO) and its acid-functionalized derivatives, such as sulfonated graphene oxide (SGO), were deemed as adequate fillers to improve the proton conductivity of PBI-based membranes [17–20]. The large number of oxygenated functional groups grafted on the GO pseudo-2D structure, such as carboxylic (–COOH) groups at the edges of the framework and hydroxyl (–OH) and epoxy (–O–) groups on the basal planes, bestows a high compatibility with the host polymer via both covalent and non-covalent bonding, as well as a satisfactory ability to transfer protons [18,21,22]. The latter feature can be further enhanced by the introduction of hydrophilic sulfonic acid (–SO_3H) groups on the carbonaceous layers, which can simulate the pendant groups responsible for the proton conduction in Nafion® [23]. Yusoff et al. [24] evaluated the effects of adding different amount of SGO, included between 0.5 and 6 wt%, on the acid retention and proton conductivity of PBI membranes. The sample containing 2 wt% of SGO filler displayed an improvement of the PA retention and a reduced swelling thanks to the good interaction between PBI and SGO, in addition to the highest proton conductivity of 0.029 S cm^{-1} at 150 °C when properly treated with PA up to an acid doping level of 11.63 mol of PA per PBI repeat unit. Devrim et al. [25] investigated four PBI/SGO composite membranes with SGO loadings of 2.5, 5, 7.5, and 10 wt% and acid doping levels ranging from 11 to 16. They observed a homogenous dispersion of SGO in the polymer matrix, an overall good thermal stability of the samples, and an improvement of PA retention with respect to bare PBI thanks to the hydrophilic groups provided by the SGO moieties. A proton conductivity of 0.136 S cm^{-1} at 180 °C was measured for the sample containing 5 wt% of SGO, which also showcased the better long-term stability due to the lowest acid leaching of 78%.

As one can infer from the reported studies, the employment of PA is still mandatory to supply PBI-based composites with a reliable medium for proton transport. However, the presence of free PA in PEMFCs could entail some disadvantages, such as the unwanted migration to the anodic side, the plasticizing effect and subsequent worsening of mechanical strength of the solid electrolyte, and corrosion phenomena comprehending the whole system [26–28]. Moreover, the benefits of PA doping in terms of conductivity improvement become effective at 150–200 °C. Contrarily, there exists a visible shortage of materials able to adequately operate within the temperature range of 80–120 °C, which is therefore recognized as the “conductivity gap” [29,30]. At such operating parameters, the device would profit from the use of a less purified fuel, a faster reaction kinetics, and an easier water management [31].

This work aspires to fill this “conductivity gap” by proposing the design of innovative composite membranes based on a combination of PBI and SGO with mass contents of the latter never explored in the literature, such that the PA doping to reach satisfactory performances in the above-stated conditions could be avoided. A set of five different samples with PBI-to-SGO mass ratios equal to 3:1, 2:1, 1:1, 1:2, and 1:3, i.e., with SGO mass contents ranging from 25 wt% to 75 wt%, was fabricated through a lab-designed method based on solution casting. The morphological, microstructural, and thermal features of the target composites were examined through surface and cross-sectional scanning electron microscopy (SEM), X-ray diffraction (XRD), attenuated total reflection Fourier-transform infrared spectroscopy (ATR-FTIR), and thermogravimetric analysis (TGA). Moreover, the effect of the diverse SGO loadings on both composites-water interplay and swelling ratio were investigated through water immersion tests. Concerning the evaluation of proton conductivity, electrochemical impedance spectroscopy (EIS) tests at 60, 80, 100, and 120 °C were performed both in the in-plane and through-plane directions, also assessing the anisotropy of proton transport driven by the structure of the composites. The gathered experimental results, compared with the ones of benchmark membranes of pristine PBI and SGO, allowed to verify the feasibility and reproducibility of the designed preparation procedure, as well as to comprehend how the interactions between the two constituents affected the structural and functional properties of the novel PBI/SGO composite membranes.

2. Experimental

2.1. Materials

PBI in powdered form (chemical structure $(C_{20}H_{12}N_4)_n$, $T_g \approx 425$ °C, $T_d > 600$ °C, brownish wool-like texture) was supplied by Blue World Technologies Aps (Aalborg, Denmark) under the trade name of Dapozol® PBI. The average molecular mass was 93,000 g mol^{-1} and the relative density at 23 °C was 1.30 g cm^{-3}.

A 0.4 wt% aqueous dispersion of GO was acquired from Graphenea, Inc. (Cambridge, MA, USA). It was characterized by a monolayer content >95 %, an average particle dimension of 600 nm, and a pH between 2.2 and 2.5.

Sigma-Aldrich (Burlington, MA, USA) provided concentrated sulfuric acid (H_2SO_4, ACS reagent, purity of 95.0–97.0%), liquid dimethyl sulfoxide (DMSO, chemical structure C_2H_6OS), and polyvinylidene fluoride (PVDF) filter disks (Durapore®, pore size of 0.22 μm, thickness of 125 μm).

2.2. Composite membranes design and preparation

The workflow to prepare the innovative PBI/SGO composite membranes (Fig. 1), characterized by PBI-to-SGO mass ratios significantly higher than those typically explored in the literature, was designed by combining a conventional solution casting method [17,20,24,32–34] with a GO sulfonation process developed elsewhere [23].

In step (A), raw PBI powder was grinded in an Agate mortar and dissolved at 2 wt% concentration in DMSO by heating at 100 °C (±2 °C) for 2 h under magnetic stirring. In step (B), GO was sulfonated by adding H_2SO_4 to the ultrasonicated GO aqueous dispersion in a H_2SO_4-to-GO molar ratio equal to 10, according to the procedure discussed by a previous work [23] and involving magnetic stirring for 3 h at 25 °C (±2 °C), followed by 3 h at 100 °C (±2 °C). In step (C), the sulfonated graphene oxide (SGO) dispersion was vacuum filtered for 2 h through a PVDF filter disk placed in a Büchner funnel. During the process, a total of 300 mL of deionized water was progressively poured into the funnel to dilute the dispersion and to remove possible unreacted acid in excess. At the end of filtration, a paste-like compound was recovered and subjected to a mild oven-drying at 40 °C to evaporate residual water. In step (D), 1 wt% SGO was incorporated in DMSO through 45 min of ultrasonication and additional 3 h of magnetic homogenization at room temperature. In step (E), the proper amounts of PBI-in-DMSO solution and SGO-in-DMSO solution were homogenously mixed up by vigorous stirring for 3 h at room temperature to obtain a PBI/SGO solution. In the last step (F), casting of the PBI/SGO solution onto a 7 cm-Petri dish and oven-drying at 90 °C for 3–5 h were performed to foster the self-assembly of the PBI/SGO composite membranes, whose tentative schematic structure is shown in Fig. 2. Such temperature was chosen to avoid unwanted thermal reduction of the GO layers, which could occur above 100 °C [35].

To ensure comprehensiveness, pure PBI and pure SGO samples were

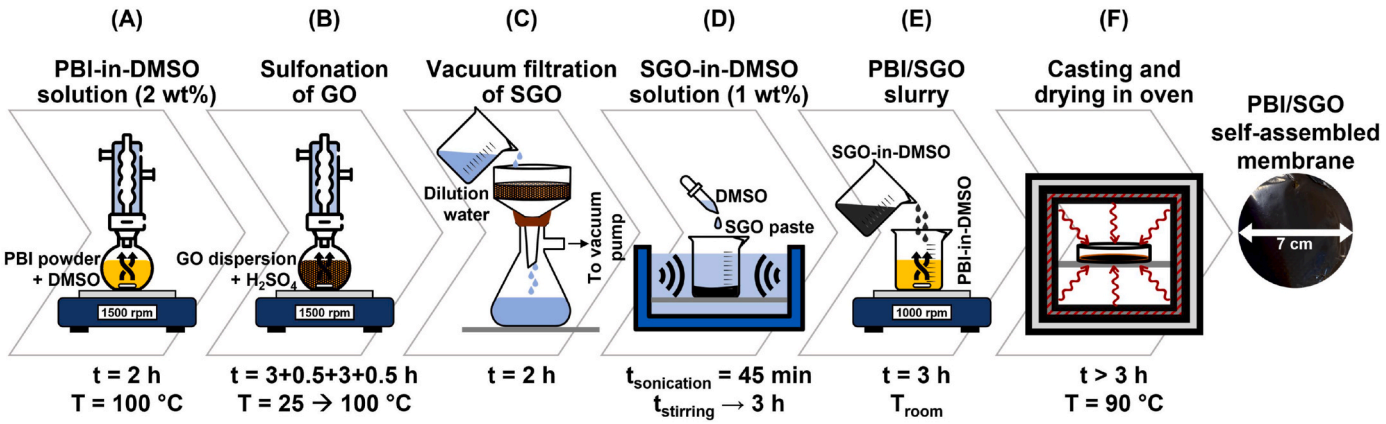

Fig. 1. Designed steps for the preparation of the PBI/SGO composite membranes.

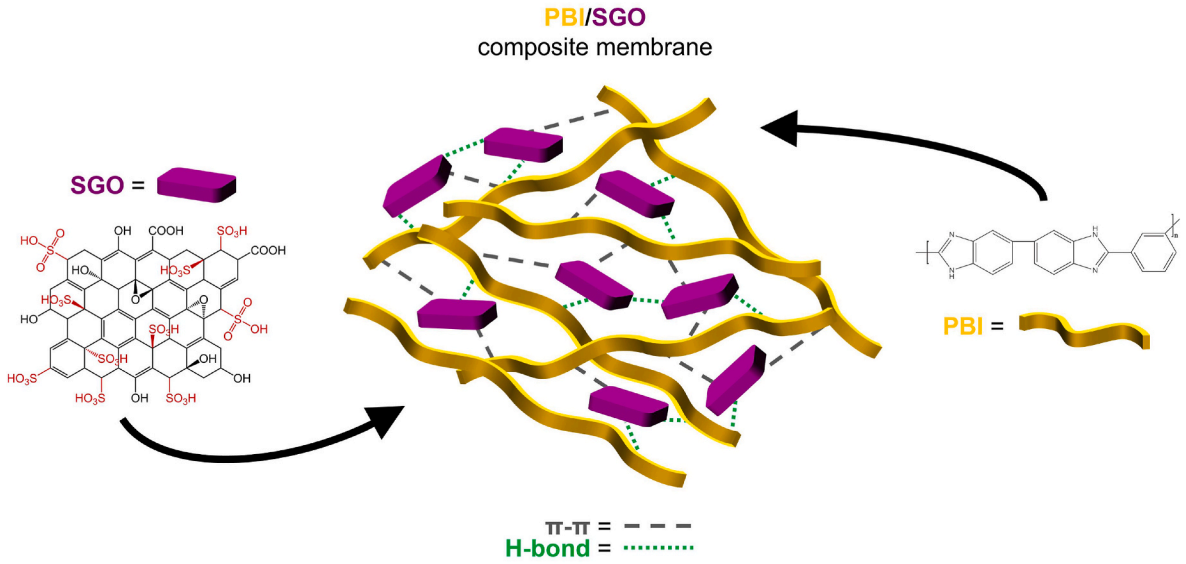

Fig. 2. Schematic chemical structure of the PBI/SGO X:Y composite membranes.

prepared and characterized as benchmarks. The production of the pure PBI membrane involved the previously described steps (A) and (F), i.e., dissolution of the fine PBI powder in DMSO, casting of the solution onto a 7 cm-Petri dish, drying for 3 h, and final detachment from the support. Concerning pure SGO, its preparation was based on the steps (B) and (C), after which the deposit at the bottom of the Büchner funnel was oven-dried at 40 °C for a few hours, until the removal of water and the complete self-assembly of the pristine SGO membrane.

As reported in Table 1, the samples fabricated and investigated in this work had PBI-to-SGO mass ratios of 3:1, 2:1, 1:1, 1:2, and 1:3. One of the purposes was to illustrate the viability of manufacturing self-assembling membranes possessing a SGO mass content ranging from a minimum of 25 wt% (3:1 mass ratio) to a maximum of 75 wt% (1:3 mass ratio), one order of magnitude greater than what is typically reported in the literature [20,24,25]. The samples were named PBI/SGO X:Y, where X:Y stands for the specific PBI-to-SGO mass ratio. An attempt to control the final thickness of the set of composite membranes was made by fixing the total mass of both constituents at 0.25 g.

2.3. Composite membranes characterization

Scanning electron microscopy (SEM) images of both surface (5000× magnification) and cross-section (1000× magnification) of the as-prepared PBI/SGO composite membranes were acquired by the

Table 1
Quantities of PBI, SGO, and their DMSO solutions according to the respective X:Y mass ratios.

Sample	PBI mass (g)	PBI-in-DMSO 2 wt% solution (g)	SGO mass (g)	SGO-in-DMSO 1 wt% solution (g)
PBI	0.25	7.50	–	–
PBI/SGO 3:1	0.1875	9.375	0.0625	6.25
PBI/SGO 2:1	0.1667	8.333	0.0833	8.333
PBI/SGO 1:1	0.125	6.25	0.125	12.50
PBI/SGO 1:2	0.0833	4.165	0.1667	16.67
PBI/SGO 1:3	0.0625	3.125	0.1875	18.75
SGO	–	–	0.25	–

microscope model 7900F by JEOL, Ltd (Tokyo, Japan). As a preliminary step, the samples were placed on a dual-sided carbon tape, fixed to a holder, and then coated by a 20-nm gold film. Subsequently, the images were taken under the following operating conditions: chamber pressure of 9.6 10^{-5} Pa, accelerating voltage of 5 kV, and a maximum current probe of 70 μA.

The diffractometer model D8 Advance by Bruker Corporation (Billerica, MA, USA) was used for the X-ray diffraction (XRD) analysis aimed at checking the crystallinity or the amorphous characteristics of the different composites, pure PBI, and pure SGO. The instrument exploited the K-α radiation with a wavelength of 1.54 Å emitted from a copper filament, collimated, concentrated, and then filtered by a graphite monochromator. A scanning rate of 0.02° per second with a count time of 3 s was employed in the $2° < 2\theta < 30°$ angular interval.

Fourier-transform infrared (FTIR) spectroscopy experiments were performed on the PBI/SGO composite membranes under macro attenuated total reflection (ATR) mode using the Thermo Nicolet iN10 MX spectrometer supplied by Thermo Fisher Scientific Inc. (Rodano, Italy). A single reflection silicon crystal, combined with a mercury cadmium telluride (MCT) detector cooled by liquid nitrogen (≈77 K), was used for the setup. For each sample, several measurements were taken within a wavenumber interval of 4000–650 cm^{-1} (mid infrared region) with a resolution of 4 cm^{-1} and 128 scans.

The thermal properties of the PBI/SGO membranes were studied using the EXSTAR 6000 TG/DTA 6300 by Seiko Instruments Inc. (Chiba, Japan). The thermogravimetric analysis (TGA) was performed by fluxing 55 mL min^{-1} of pure nitrogen and by applying a temperature ramp with a constant heating rate of 10 °C min^{-1} from 30 °C to 800 °C. During the tests, the mass loss was monitored through an electronic microbalance. The corresponding residual mass percentage as a function of the temperature underlined the occurrence of structural modification of the investigated materials.

2.4. Water immersion tests

The purpose of the lab-designed water immersion tests was to evaluate the water retention capability of the PBI/SGO X:Y, benchmark PBI, and benchmark SGO membranes, as well as to estimate if and to which extent they could sustain an aqueous environment for a long time. Accordingly, the duration of the experiments was set to 3 months. Preliminarily, all the samples were oven-dried for 2 h at 60 °C to remove any trace of moisture and to measure their dry mass (m_{dry}, mg). Each dried sample was immersed in a separate beaker containing 200 mL of deionized water. The beakers were then properly sealed with parafilm tape.

The wet mass (m_{wet}, mg) values were acquired at timesteps of 2 days, 1 week, 2 weeks, 1 month, 2 months, and 3 months. The procedure involved the extraction of the samples from their beaker, the careful dabbing with paper towel on both surfaces for 30 s to remove the excess of water and, eventually, the weighing on an analytical balance. Eq. (1) was used to determine the mass increase (MI, %) due to water absorption:

$$MI = \frac{m_{wet} - m_{dry}}{m_{dry}} \cdot 100 \quad (1)$$

The tests also allowed to assess the long-term swelling ratio (SR, %) of the membranes through Eq. (2). This quantity provided a numerical estimation of the tendency of the composites to swell upon soaking, which should be minimal to prevent any possible mechanical criticality in a fuel cell assembly. The dry thickness (t_{dry}, μm) before immersion and the wet thickness (t_{wet}, μm) at the end of the 3-months experiments were measured with the digital Fujisan 0–25 mm (±1 μm) micrometer:

$$SR = \frac{t_{wet} - t_{dry}}{t_{dry}} \cdot 100 \quad (2)$$

2.5. Electrochemical impedance spectroscopy

Electrochemical impedance spectroscopy (EIS), performed in a lab-designed humid chamber at 60, 80, 100, and 120 °C under 95% RH, was executed to assess the proton conductivity of the PBI/SGO X:Y composite membranes. Rectangular samples (40 mm length x 10 mm width), properly trimmed from each prepared membrane, were dried for 2 h at 60 °C to measure their dry thickness (t_{dry}, μm). The samples were fastened to an inert Teflon® cell, which was assembled with two stainless steel electrodes and inserted in the chamber, filled with 0.6 L of deionized water, for 1 h. Temperature control was ensured with continuous recirculation of heated oil in the outer shell of the chamber and with the insertion of a thermocouple in the system. Three measurements for each sample were collected by means of the Bode Analyzer tool of STEMlab™ 125–14 by Red Pitaya (Solkan, Slovenia) to check repeatability. The instrument was connected to an interface laptop, to a resistive element, and, ultimately, to the stainless-steel electrodes by means of cables and clips necessary to close the circuit. The Bode Analyzer was used in potentiostatic mode in the frequency range 1–10^7 Hz with a signal amplitude of 1 V. The gathered Bode diagrams were converted into Nyquist plots and analyzed using the ZView® software (Scribner Associates Inc., Southern Pines, NC, USA). The average values of the internal resistance (R_i, Ω) were computed by choosing the most suitable equivalent circuit to describe the studied electrochemical system [36,37].

In PEMFCs, the protons can be transported in two different directions, along the membrane and through the membrane. Coherently, in this work EIS analyses were performed with two different Teflon® cell configurations (Fig. 3). In the in-plane configuration (Fig. 3(a)), the two electrodes clamped the rectangular sample at its extremities. The corresponding in-plane proton conductivity (σ_{in}, S cm^{-1}) values were computed through Eq. (3), in which w_1 (cm) is the width of the sample and d_1 (cm) is the distance between the electrodes:

$$\sigma_{in} = \frac{d_1}{w_1 \cdot t_{dry} \cdot R_i} \quad (3)$$

The through-plane configuration (Fig. 3(b)) was appositely designed to sandwich the specimen between the two electrodes. The corresponding through-plane proton conductivity (σ_{th}, S cm^{-1}) values were determined via Eq. (4), where the product $w_2 \cdot d_2$ (cm^2) is the contact area of the electrodes:

$$\sigma_{th} = \frac{t_{dry}}{w_2 \cdot d_2 \cdot R_i} \quad (4)$$

The dimensionless anisotropy factor (AF), calculated with Eq. (5) as proposed by Luo et al. [38], was exploited to verify the relationship between the in-plane and through-plane proton conductivities of the PBI/SGO X:Y composite membranes and, hence, to understand whether the transport of protons within the membranes occurred in a preferential direction:

$$AF = \frac{\sigma_{in} - \sigma_{th}}{\sigma_{in} + \sigma_{th}} \quad (5)$$

3. Results and discussion

3.1. Composite membranes

Fig. 4 displays the macroscopic aspect of the PBI/SGO X:Y composite membranes, as well as pure PBI and pure SGO samples for comparison purposes. Several considerations were included in the rationale behind the design of the preparation procedure, whose aim was the fabrication of innovative self-assembling membranes in which PBI and SGO were combined with mass ratios never explored in previous works. In the first place, safety was a matter of concern. From a literature review, N,N-dimethylformamide (DMF) and, especially, N,N-dimethylacetamide

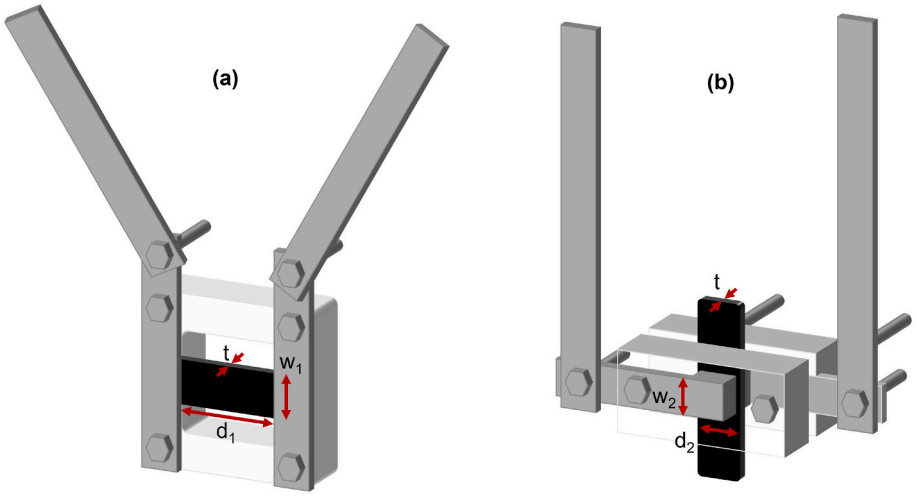

Fig. 3. Teflon® cell configurations designed for evaluating (a) in-plane proton conductivity and (b) through-plane proton conductivity.

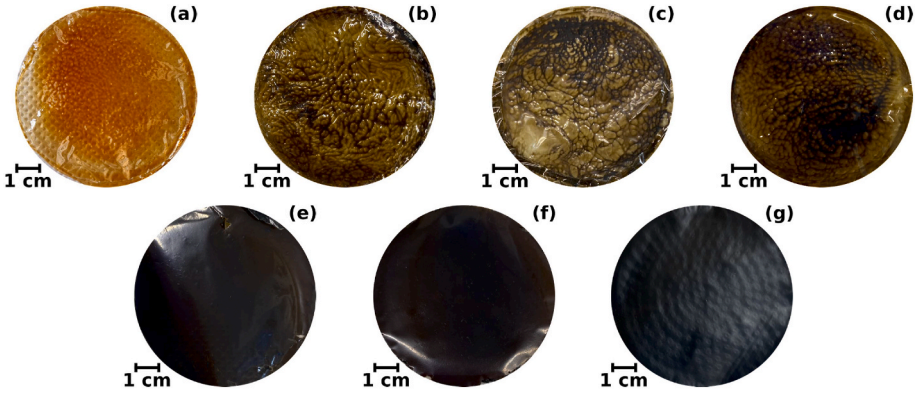

Fig. 4. Macroscopic aspect of: (a) pure PBI membrane, PBI/SGO composite membranes with mass ratio of (b) 3:1, (c) 2:1, (d) 1:1, (e) 1:2, (f) 1:3, and (g) pure SGO membrane.

(DMAc) were identified as the preferred solvents employed in solution casting methods for the preparation of PBI-based membranes [5,17,19,20,24,33]. However, these species are renowned for their toxicity and hazardousness, especially toward human health, motivating the research for different options. With these premises, safety was pursued by opting for DMSO as the organic solvent of the designed procedure. This aprotic and highly polar solvent was demonstrated to be much less toxic than other commonly used species [39,40]. Furthermore, it highlighted a remarkable compatibility with both constituents, inasmuch its Hansen solubility parameter (HSP), which commonly describes the solute-solvent mutual affinities, was comparable with the ones identified for PBI and GO-related materials [41–43].

The second condition to be fulfilled was reproducibility of the newly developed procedure. It was attained by means of the optimization of each of the steps described in Section 2.2, specifically in terms of the employed quantities and the operating conditions. In detail, the optimal amounts ensuring the proper dissolution in DMSO were determined to be 2 wt% for PBI at 100 °C and 1 wt% for SGO at room temperature. The impossibility to execute SGO dissolution in DMSO at high temperature derived from the intention to preserve the oxygenated functionalities of GO. The exposure of GO to temperatures of ≈100 °C could cause an unwanted reduction of the basal planes, with the subsequent loss of proton conductive functional groups [35]. This precaution was extended to the solvent evaporation step as well, for which an operating temperature of 90 °C was configurated. The downside was a temporal extension of steps (D) and (F). Despite this, the designed workflow was highly reproducible, and several stable samples were accordingly prepared for each investigated PBI-to-SGO mass ratio.

The different SGO contents in the composites clearly resulted in a gradual alteration of their overall appearance. In PBI/SGO 3:1 (Fig. 4(b)), dark brown veins attributed to SGO were observed in the PBI matrix. Regardless, the optical transparency typical of PBI membranes (Fig. 4(a)) was preserved. For higher SGO concentrations, the transparency of the samples progressively diminished, indicating a positive coexistence of the two constituents [44]. In PBI/SGO 1:2 (Fig. 4(e)) and PBI/SGO 1:3 (Fig. 4(f)), the SGO loading (66 wt% and 75 wt%, respectively) became dominant over PBI, implicating a highly homogenous and blackish texture, akin to that of the pure SGO membrane (Fig. 4(g)).

The thicknesses of the PBI/SGO X:Y composite membranes were in the order of tens of μm, as shown in Table 2. Despite the attempt of thickness control via fixing the total mass of the constituents, the samples with higher SGO contents resulted to be thinner. Values closer to that of pure SGO, displayed by PBI/SGO 1:2 and PBI/SGO 1:3, probably

Table 2
Average thicknesses of the PBI/SGO composite membranes and benchmark PBI and SGO membranes.

	PBI	PBI/SGO 3:1	PBI/SGO 2:1	PBI/SGO 1:1	PBI/SGO 1:2	PBI/SGO 1:3	SGO
Thickness (μm)	58 ± 7	49 ± 10	51 ± 13	29 ± 5	18 ± 4	22 ± 9	12 ± 0.1

originated from the better packing of the SGO moieties, in excess with respect to PBI. Nonetheless, the average thickness values were consistent with those found in the literature and close to the one of commercial proton exchange membranes [8].

3.2. Composite membranes characterization

Fig. 5 gathers (1) the surface SEM images at 5000× magnification and (2) the cross-sectional SEM images at 1000× magnification of the PBI/SGO X:Y composite membranes, pristine PBI, and pristine SGO. The composites proved to be homogeneous and uniform, without any macroscopic defect, crack, or cavities. PBI/SGO 3:1 (Fig. 5(b-1)), 2:1 (Fig. 5(c-1)), and 1:1 (Fig. 5(d-1)) displayed a more planar and smoother surface resembling the pure PBI membrane (Fig. 5(a-1)), consistently with literature observations [30,44]. Additionally, darker stripes were perceived in PBI/SGO 3:1. This feature was consistent with the vein-like SGO distribution observed from the macro-morphology of the samples. Compared to the other composites, the surfaces of PBI/SGO 1:2 (Fig. 5 (e−1)) and 1:3 (Fig. 5(f-1)) appeared to be more wrinkled. SGO contents of 66 wt% and 75 wt%, respectively, involved a larger presence of oxygenated functionalities and sulfonic acid groups. The corresponding hydrogen bonding interactions likely caused framework tensions that promoted a higher degree of disorder, a trait further emphasized in the pure SGO membrane [23,25,45]. Such a variation of the surface features of the composites, relative to the progressive increase of the SGO concentration, remarked the good compatibility of PBI and SGO moieties and the reliability of the designed preparation procedure.

From the cross-sectional standpoint, PBI/SGO 3:1 (Fig. 5(b-2)) and 2:1 (Fig. 5(c-2)) were compact and homogenous, again in a similar fashion to PBI (Fig. 5(a-2)) [19,26,46]. In the situation of PBI predominance within the composites structure, SGO sheets remained dispersed and exfoliated at the microscopic level in the polymer matrix. The highest SGO concentration in PBI/SGO 1:3 (Fig. 5(f-2)) provoked the appearance of some small clusters, associated to the establishment of hydrogen bonds among adjacent flakes. Differently, the multilayer structure of pure SGO arose from the production procedure, which implied the continuous stacking of single layers during vacuum filtration until the self-assembly of the membrane [12]. The SEM investigation of cross-sections allowed to confirm the trend reported in Table 1, according to which the membranes with higher SGO content showed lower average thicknesses.

The X-ray diffractograms acquired for the PBI/SGO X:Y composite membranes and benchmark PBI are depicted in Fig. 6(a). In PBI-based membranes, a low-intensity broad contribution falling within the $20^\circ < 2\theta < 30^\circ$ interval is typical. It can be related to the convolution of the amorphous and semi-crystalline fractions of the polymer, due to which adjacent benzimidazole chains arrange in a face-to-face configuration [17,24,30,47]. Such a feature was coherently observed in the patterns of the PBI/SGO X:Y composite membranes and pure PBI. The main difference regarded the conformation of the broad contribution, which resulted to be left-shifted for the composites with respect to pure PBI (black dotted region in Fig. 6(a)). The onset of such a deviation even at the PBI-to-SGO mass ratio of 3:1, thus at the lowest SGO mass content (25 wt%), implied an increase in the reciprocal distance between the polymeric chains due to the incorporation of SGO flakes.

As the concentration of SGO increased, a contribution at lower 2θ angles began to emerge (red dotted region in Fig. 6(a)). This feature agreed with the diffractogram of pure SGO, reported in Fig. 6(b), whose major characteristic was the sharp diffraction peak at $2\theta \approx 8^\circ$. According to the Bragg's law, the corresponding interplanar distance was approximately 11 Å, larger than the one of pure GO (8–9 Å [32,42,47]). The sulfonation process (step (B) in Fig. 1) caused an increase of the interlayer spacing due to the grafting of $–SO_3H$ groups on the GO framework, equally preserving its crystallinity (001-diffraction plane). However, the SGO reflections in the PBI/SGO X:Y samples were broader and less sharp compared to the pure sample. This outcome was attributed to the

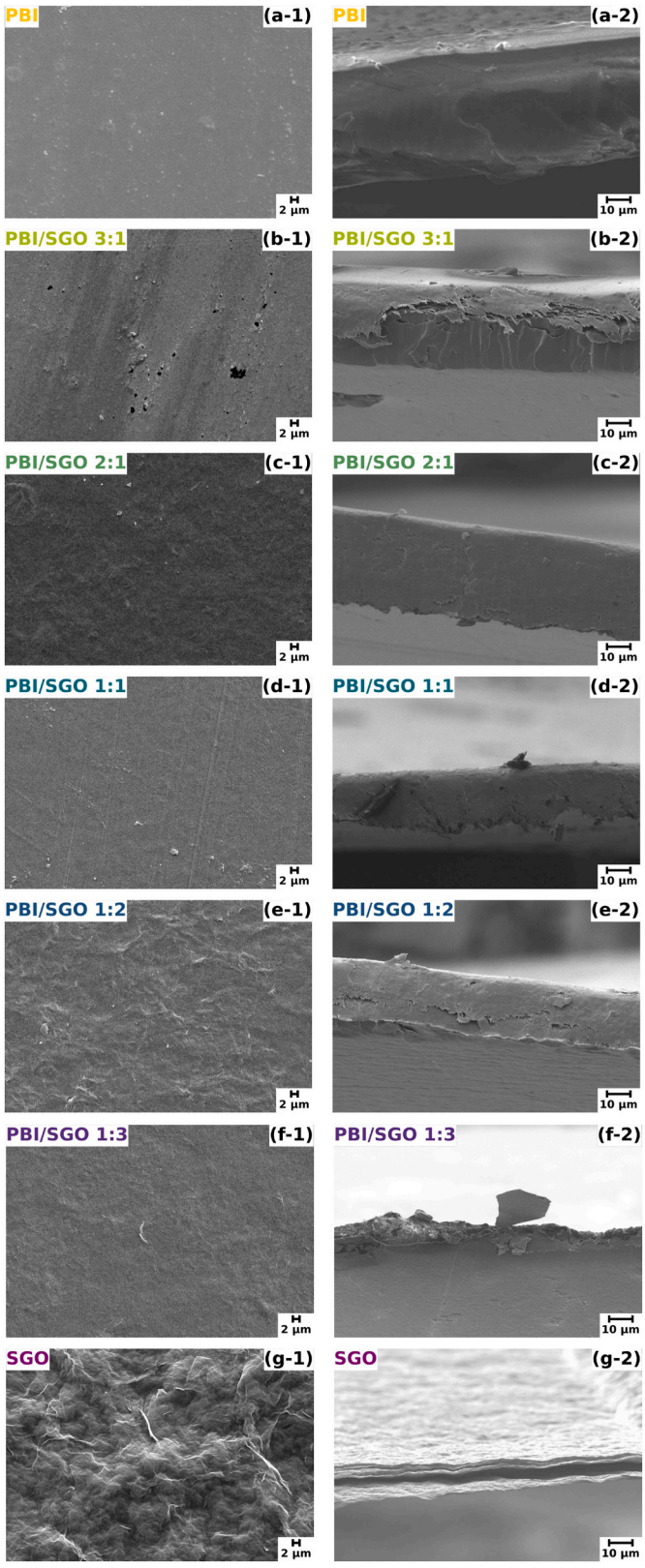

Fig. 5. 5000×-magnified surface (set 1, left column) and 1000×-magnified cross-sectional (set 2, right column) SEM images of (a) pristine PBI, (b–f) PBI/SGO X:Y samples, and (g) pristine SGO.

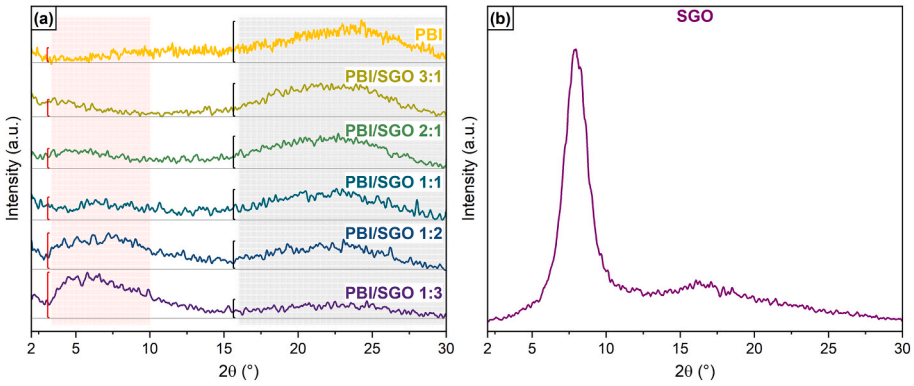

Fig. 6. Diffractograms of (a) the fabricated PBI/SGO X:Y composite membranes and reference PBI, (b) benchmark SGO.

predominant amorphous character of the composite membranes, resulting from the exfoliation of the SGO flakes within the PBI matrix previously observed from cross-sectional SEM. The higher intensity of the SGO contribution for PBI/SGO 1:2 and 1:3 was likely related to the larger and prevailing presence of SGO moieties. The only partial loss of transparency appreciated in the macroscopic inspection supported this hypothesis. In the broader context of proton exchange membranes, the proton conduction is said to mainly occur within the amorphous phase. The regular atomic arrangement and long-range order found in the crystalline phase is indeed expected to hinder the proton movement [47,48]. Therefore, the PBI/SGO X:Y composite membranes might exert the transport of protons through their mainly amorphous structure.

Altogether, the accentuated appearance of an SGO contribution at larger SGO contents (i.e., in PBI/SGO 1:2 and 1:3) was coherent with the unexplored mass ratios tested in this work, since no discrete and sharp peaks were observed in other works, suggesting that low SGO mass contents did not involve changes in the PBI arrangement [20,24,46]. Moreover, the slight shift of both PBI and SGO contributions toward smaller diffraction angles provided promising evidence of the effective self-assembly process of the membranes, again highlighting the reciprocal compatibility between the two constituents.

Fig. 7(a) shows the ATR-FTIR spectra of benchmark PBI and SGO, which were compared to the spectra acquired for the PBI/SGO X:Y composite membranes in Fig. 7(b). The outcomes appeared to again indicate an effective combination of PBI and SGO through the designed preparation procedure. PBI/SGO X:Y samples displayed an array of contributions very similar to that of pure PBI, whose spectrum was consistent with existing literature [49]. The broad bands (a) at 3400 cm^{-1} and (b) at 3200 cm^{-1} were assigned to the free non-hydrogen bonded N–H stretching and to the combination of self-associated N–H stretching and –OH stretching vibrations, respectively. Three contributions (c) could be detected at 1629, 1610, and 1590 cm^{-1}, referable to the stretching vibrations typical of conjugation between imidazole and benzene rings, i.e., C=N, C=C, and ring vibration, respectively. The band (d) at 1532 cm^{-1} was consistent with the in-plane deformation of benzimidazole, the one (e) at 1438 cm^{-1} was attributed to the in-plane vibration of 2,6-disubstituted benzimidazole, and the characteristic one (f) at 1280 cm^{-1} was related to the C–N stretching vibrations in the imidazole moieties. Lastly, the contribution (g) at 1012 cm^{-1} was assigned to benzene ring vibration, whereas the band (h) at 801 cm^{-1} was attributed to the heterocyclic ring vibration.

Some peculiar differences could be ascribed to the combination with SGO, which demonstrated expected features as well when investigated in pristine form [12,23]. A slight reduction (downwards arrows) in the intensity of the broad bands (a) and (b) was explained by the possible hydrogen bonding between the N–H groups of PBI strands and the oxygen-containing functional groups decorating SGO, owing to which the amount of hydrogen bonds among PBI moieties diminished. At the same time, a progressive reduction of the intensity of the bands (e), (f), and (h), distinctive of PBI, was detected as the SGO content in the membrane became dominant. Moreover, small shoulders (k) at 1728 cm^{-1}, related to the C=O stretching from carboxyl and carbonyl groups of SGO, and (n) at 1035 cm^{-1}, ascribed to the C–OH stretching, gradually appeared as the SGO mass content became larger (upwards arrows). Likely due to the overlap with the multiple bands of PBI, other characteristic contributions assigned to the GO framework (the combination of the –OH stretching in hydroxyl functionalities, carboxylic acid groups, and adsorbed water (i), the C=O stretching in anhydride groups (j) at 1818 cm^{-1}, the O–H bending within adsorbed water molecules (l) at 1615 cm^{-1}, and the stretching of covalent bonds in tertiary alcohols (o) at 981 cm^{-1}) and to the presence of sulfonic acid groups (the stretching vibration of the O=S=O bonds in sulfonic acid groups (m) at 1160 cm^{-1} and the S–O stretching in sulfonic and sulfinic acid groups (p) at roughly 880 cm^{-1}) could not be unambiguously identified in the composite

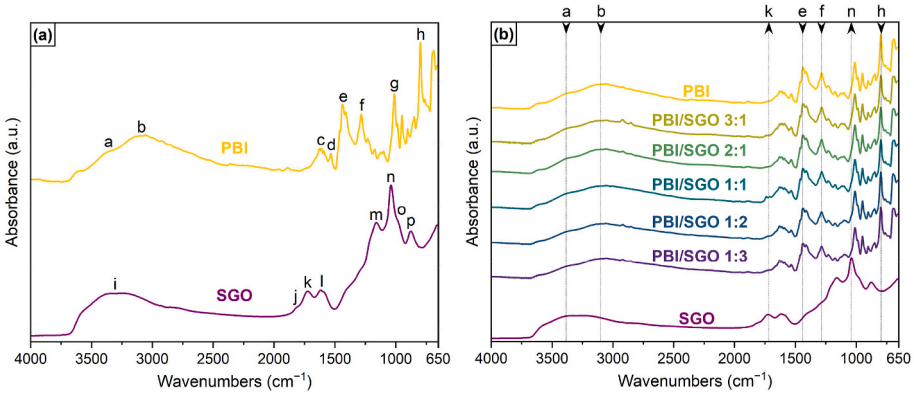

Fig. 7. (a) ATR-FTIR spectra of pure PBI and pure SGO; (b) comparison with the ATR-FTIR spectra of the PBI/SGO X:Y composite membranes.

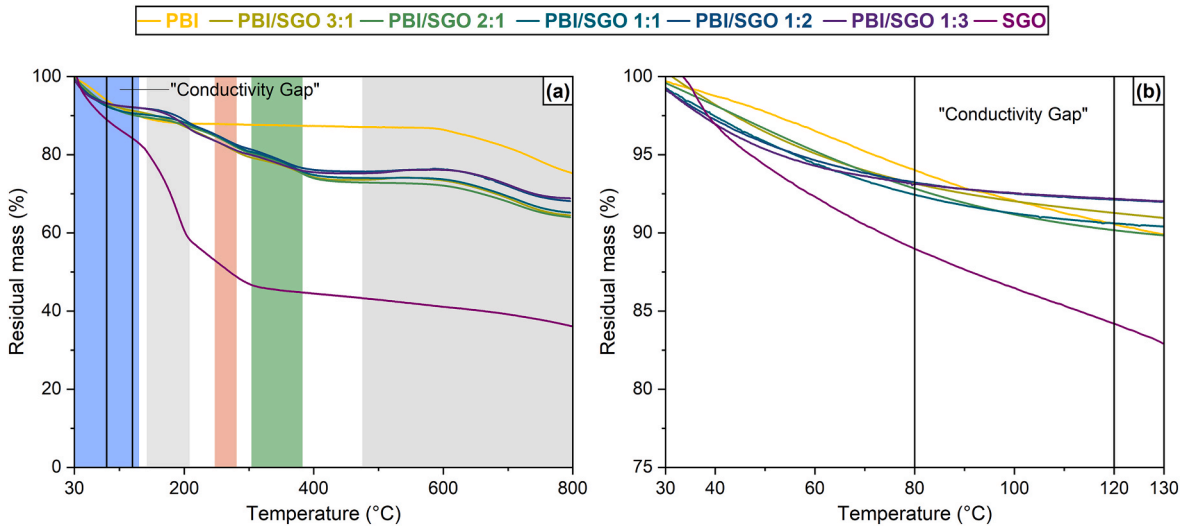

Fig. 8. (a) Thermograms of the PBI/SGO X:Y composite membranes, pristine PBI, and pristine SGO membranes; (b) close-up of the thermal behavior of the samples within the 30–130 °C temperature range.

membranes spectra.

The thermograms of the PBI/SGO X:Y composite membranes, pure PBI, and pure SGO are illustrated in Fig. 8(a). The composite membranes underwent five mass losses, in contrast to the four-stage mass loss of pure SGO and the three-stage mass loss of pure PBI. The first mass loss (blue) was common to all the samples. It can be related to the elimination of physically adsorbed water molecules [5,23,44], and, to a minimal extent, to the removal of residual traces of solvent coming from the preparation procedure of the composites [20,26]. Such a mass loss was about 15% in the SGO thermogram, while it was limited to 8–10% for the composites, as well as for pure PBI. The outstanding thermal stability of the PBI chains, which might have further improved the water-holding capability of the hydrophilic SGO sheets, could justify the enhanced moisture retention of the composites with respect to benchmark SGO. Interestingly, the residual mass of the composites was almost 90% within the "conductivity gap" (i.e., between 80 and 120 °C in the close-up reported Fig. 8(b)), with no thermal phenomena attributable to molecular structure features. Such an outcome can be promising in the perspective of an application as proton exchange membranes working in such a temperature range.

In the second mass loss stage (light grey), occurring roughly between 150 and 200 °C and absent in pure PBI, the labile oxygen-containing functional groups within the SGO layers began to decompose. The composites (≈5% mass loss) witnessed a greater thermal stability than pure SGO (≈30%) in this temperature range. The hydrogen bonding interactions formed between the oxygenated moieties of SGO and PBI chains, inferred from ATR-FTIR spectra, stabilized the former within the composite membranes framework and partially hampered their decomposition. The third stage (orange) appeared between 250 and 300 °C in both composites (≈7% mass loss) and SGO (≈11% mass loss). It corresponded to the decomposition of sulfur-containing functionalities, which suggested both the efficacy of the GO sulfonation and the successful incorporation of SGO in the composites. An additional, mild mass drop (green) was detected between 300 and 380 °C in both pure PBI and composites. It was mainly attributed to the disruption of N–H and –N = groups belonging to the PBI imidazole framework [20,30]. The fifth and last stage (dark grey) highlighted a progressive mass loss between 7% and 10% for all the samples. It resulted from a combination of the pyrolysis of the graphitic planes of SGO, occurring at temperatures higher than 550 °C [12], and the degradation of carbonaceous PBI backbone chains, starting above 600 °C [25]. After the thermogravimetric experiments, the residual masses of the PBI/SGO X:Y composite membranes were found to be above 60%, independently of their PBI-to-SGO mass ratio. Such results demonstrated their superior thermal stability compared to pure SGO, which retained only 35% of its mass, due to the strong influence of the thermally resistant polymer strands. PBI/SGO 1:2 and 1:3 were able to maintain approximately 92–95% of their mass at 120 °C and 70% at 800 °C, the best performance among all the investigated composites.

3.3. Water immersion tests

The percentage mass increase (MI) and long-term swelling ratio (SR) of the PBI/SGO X:Y composite membranes, pure PBI, and pure SGO after the water immersion tests are represented in Fig. 9. Throughout the duration of the experiments, the composites and pure PBI proved an outstanding durability in the aqueous environment. The water retention capability of the PBI/SGO X:Y composite membranes kept enhancing with the progressive increase of SGO content, until reaching a plateau after 30 days due to complete saturation.

At whichever PBI-to-SGO mass ratio, the PBI strands and SGO flakes within the composites seemed to work synergistically toward the improvement of their properties. On one hand, the great endurance of PBI to the exposure to the aqueous environment prevented any type of damage to the membranes, since they were retrieved as intact after the 3

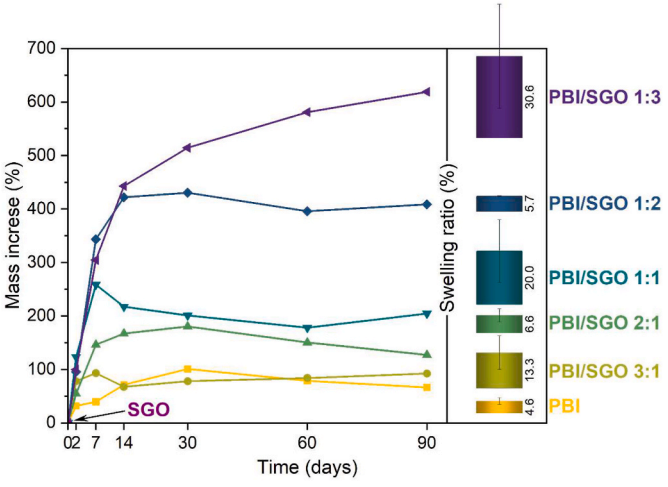

Fig. 9. Mass increase and swelling ratio results of the PBI/SGO X:Y composite membranes, pure PBI, and pure SGO.

months-long experiments. Such an outcome was in contrast with the behavior of pure SGO, which completely disintegrated after just two days of testing. The reason may lie within the high hydrophilicity of the oxygen-containing and sulfonic acid groups of SGO [50], which promoted the extensive sorption of water molecules. Nonetheless, the uncontrolled accumulation facilitated the disruption of the close-packing of SGO flakes, which, in turn, led to a more water-susceptible material and, therefore, to a fast breakdown. On the other hand, SGO enhanced the water-holding ability of the composites, even at the lowest mass ratio. Indeed, compared to pure PBI (MI = 66%), PBI/SGO 3:1 reached a larger value of 92%. Then, progressive improvements were recorded up to the best performance guaranteed by PBI/SGO 1:3 (MI = 619%). This trend derived from the larger quantity of hydrophilic functionalities introduced by the SGO framework within the composites, raising their ability to interact with water via hydrogen or electrostatic bonds. Such a behavior could play a crucial role for the proton conductivity of the samples, since water can serve as a carrier for proton transport [8,10,47].

Despite the remarkable response to soaking, the PBI/SGO X:Y composite membranes exhibited a restrained dimensional swelling after 90 days of the lab-designed test (i.e., maximum of 30.6% observed for PBI/SGO 1:3). The intermolecular interactions formed between the functional groups of PBI and SGO, underlined by ATR-FTIR analysis, prevented an excessive polymer chain expansion [46,50]. Overall, these results demonstrated the capability of the PBI/SGO X:Y composite membranes to maintain a suitable level of water sorption together with a limited SR, necessary for the preservation of a proper proton conductivity and a good integrity of the membranes [24,32]. The best compromise between the investigated properties was observed for PBI/SGO 1:2, which exhibited a remarkable mass increase due to water soaking (409%) along with the lowest SR (5.72%).

3.4. Electrochemical impedance spectroscopy

Fig. 10 summarizes the average (a) in-plane and (b) through-plane proton conductivity values of the undoped PBI/SGO X:Y membranes extrapolated from EIS experiments. Higher temperatures involved a slight increase of the in-plane proton conductivity of the composites [6,23,47]. An enhancement with respect to pure PBI (highest σ_{in} of 0.032 S cm^{-1} at 120 °C) was recorded even for the membrane with the lowest PBI-to-SGO mass ratio (i.e., 25 wt% of SGO, highest σ_{in} of 0.042 S cm^{-1} at 120 °C), due to the positive impact of the oxygen-bearing functionalities and sulfonic acid groups. Accordingly, the increase of in-plane proton conductivity was particularly pronounced for larger SGO contents. PBI/SGO 1:2 (66 wt% of SGO) reached the best performance of 0.113 S cm^{-1} at 120 °C, which roughly corresponded to a 4-fold improvement with respect to pristine PBI. Several factors contributed to this outcome, such as the high acidity of –SO_3H groups (pKa <1), which could promote a fast reception and release of protons [20]. At the same time, the hydrogen bonding between the N–H groups of PBI and the functional groups of SGO led to the formation of new strongly interconnected proton transfer channels within the membranes [24,26]. Additionally, the hydrophilicity of –SO_3H groups allowed for a better clustering of surrounding water molecules, improving the availability of bound water and the phase separation of hydrophobic and hydrophilic zones even at temperatures exceeding 100 °C [44]. Such a behavior would agree with the water immersion tests and TGA results, according to which the composites showed a large water absorption and a great moisture retention. Even at 120 °C, no reduction phenomena of SGO and consequent proton conductivity worsening were noticed, likely due to a protective action of the thermally stable PBI on the oxygenated functionalities of SGO. In such an amorphous PBI/SGO network, as indicated by XRD analysis, a combination of Grotthuss (proton hopping) and vehicular (travel of hydronium ions) proton transfer mechanisms can be presumed, the latter more prominent at the lowest temperatures of the studied interval (i.e., 60 and 80 °C) and hinted by the previously described good interplay between membranes and water [5,50]. The slight drop observed for PBI/SGO 1:3 (0.092 S cm^{-1} at 120 °C) can be likely justified by the aggregation of some SGO clusters seen in the cross-sectional SEM images, which might have produced more tortuous pathways for proton transport. Nevertheless, the performance of the composites with large SGO contents was akin to that of Nafion® at its working temperatures (≈0.1 S cm^{-1} at 80 °C [9,15]), and an evident step up with respect to the commercial material within the operating conditions which forbid its use.

The considerations regarding the beneficial influence of temperature, content of sulfonic acid groups, and their interaction with PBI remained valid for the through-plane proton conductivities, albeit lower outcomes were obtained. PBI/SGO 1:3, whose σ_{th} was equal to 0.025 S cm^{-1} at 120 °C, guaranteed the best performance among the samples and an improvement of 108% with respect to PBI/SGO 3:1 (σ_{th} of 0.012 S cm^{-1} at 120 °C). The difference existing between proton migration in the planar and transversal directions was accounted for with the evaluation of the anisotropy factor. Fig. 11 shows the values obtained for the composites as a function of the PBI-to-SGO mass ratio and the temperature. Anisotropy is a feature generally characterizing conventional Nafion®-based membranes, as discussed in the literature [38,51,52]. Depending on the manufacturing and processing procedures, the anisotropy factor can range between 0.2 and 0.65, demonstrating a better aptitude to proton transport in the in-plane direction. The PBI/SGO X:Y composite membranes generally complied with this behavior, providing average values between 0.52 and 0.91. An inverse proportionality with temperature and a direct proportionality with SGO content were detected. In the former case, the thermal excitation (promoted with the temperature increase from 60 to 120 °C) flattened the discrepancy between σ_{in} and σ_{th} and lowered the anisotropy factor for

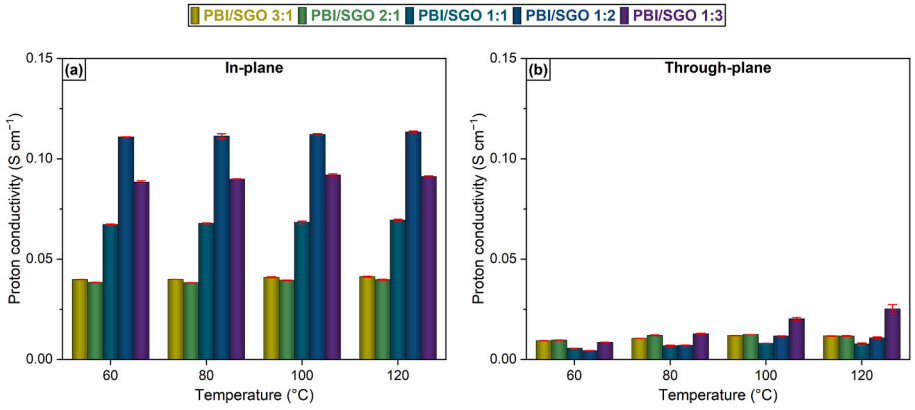

Fig. 10. (a) In-plane and (b) through-plane proton conductivity values of the PBI/SGO X:Y composite membranes.

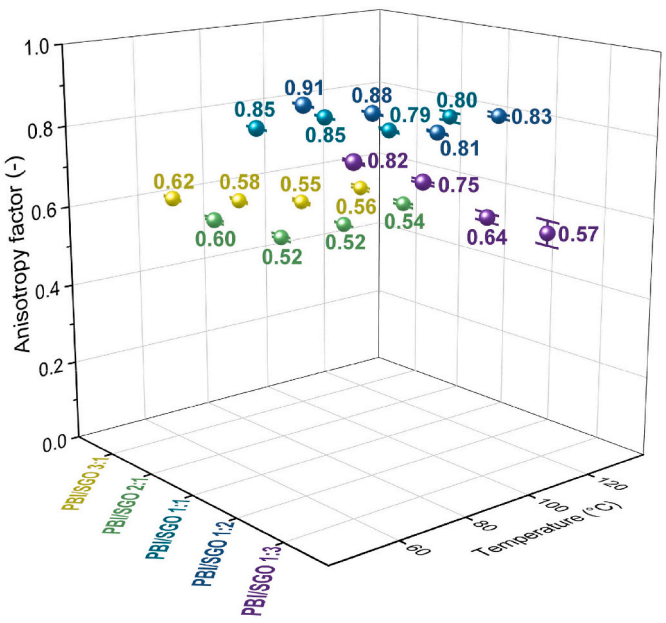

Fig. 11. Anisotropy factor of the PBI/SGO composite membranes as a function of the X:Y mass ratios and temperature.

every PBI-to-SGO mass ratio. In the latter case, higher anisotropy factors were observed for the PBI/SGO X:Y composite membranes with larger SGO loadings. This parameter influenced primarily the thickness, since thinner samples were prepared when the SGO content became dominant (see Section 3.1 and 3.2). As reported elsewhere, thinner membranes can undergo stronger interfacial effects that can influence their ability to move protons in the transversal direction [38]. Furthermore, the proton conductivity anisotropy could partially derive from the experimental setup. In this regard, the formation of highly hydrated surface layers on the samples exposed to the humid chamber with the in-plane configuration, which was instead avoided in through-plane, can be accounted for as a conditioning factor [53].

Table 3 compares the proton conductivity results of PBI/SGO 1:2 and 1:3 with state-of-the-art non-fluorinated proton exchange membranes examined in the literature. The samples studied in this work exhibited σ_{in} and σ_{th} values larger than, or at least comparable to, other materials studied in the field of proton exchange membranes. The anisotropy factors were as well consistent with the reported studies, confirming the preference for a planar proton conduction also in different non-fluorinated electrolytes. Besides, two further strong points of the PBI/SGO composite membranes with high SGO content can be elucidated. First, satisfying proton conductivity can be obtained without PA doping, which is instead mandatory in the case of PBI-based membranes. Second, the shortage of materials able to operate between 80 and 120 °C is tangible since the focus is typically put on the conventional operating temperatures of PEMFCs or on very high ones (>150 °C). Contrarily, PBI/SGO 1:2 and 1:3 demonstrated good performances in such conditions, therefore filling the "conductivity gap".

4. Conclusion

Self-assembling PBI/SGO composite membranes with innovative PBI-to-SGO mass ratios, never explored in the literature, were successfully prepared by means of a simple and reproducible lab-designed workflow. The characterization of the samples aspired to evaluate their viability as non-fluorinated proton exchange membranes working at temperatures of 80–120 °C, the so-called "conductivity gap". The use of large contents of SGO was experimented with a potential strategy for attaining satisfactory levels of proton conductivity without phosphoric acid doping, which is typical of PBI-based membranes but, at the same time, can be dangerous for PEMFCs. Surface and cross-sectional SEM revealed that larger PBI contents involved smoother surfaces in contraposition with PBI/SGO 1:2 and 1:3, which displayed wrinkled textures similar to pure SGO. The identification of both PBI and SGO contributions from XRD patterns suggested the correct combination of the constituents. Moreover, the amorphous nature of the composites was detected, a feature, which is expected to be beneficial for proton conduction purposes. TGA demonstrated the beneficial effect of thermally stable PBI, especially at temperatures lower than 120 °C, and mass losses ascribable to both species, further confirming their compresence within the composites. The excellent durability in the aqueous environment of PBI was combined with water retention, which is strongly improving with the progressive content increase of hydrophilic SGO. PBI/SGO 1:2 showed an optimal compromise between mass increase (409%) and a restrained swelling ratio of 5.72%. The EIS tests performed at 60, 80, 100, and 120 °C proved the positive impact of the hydrophilic SGO moieties, which helped the formation of hydrogen bonded pathways on both in-plane and through-plane proton conductivities. PBI/SGO 1:2 achieved the highest in-plane conductivity of 0.113 S cm^{-1} at 120 °C, whereas PBI/SGO 1:3 provided the best through-plane conductivity of 0.025 S cm^{-1} at 120 °C. The lower values observed in the transversal direction indicated the existence of a certain anisotropy of proton transfer, which resulted in a corresponding factor comprised between 0.52 and 0.91, albeit restrained values were computed at the temperatures of interest. The disclosed experimental results remarked on the promising nature of these innovative PBI/SGO composite membranes, which can contribute to filling the "conductivity gap".

Table 3
Comparison of the in-plane proton conductivity, through-plane proton conductivity, and anisotropy factor of state-of-the-art non-fluorinated membranes reported in the literature.

Membrane	σ_{in} (S cm^{-1})	σ_{th} (S cm^{-1})	Anisotropy factor (calculated)	Reference
PBI/ImGO_1.0 (PA)	0.077 @ 150 °C	–	–	[19]
N/PVA/SGO1.0	0.080 @ 25 °C	–	–	[45]
5 wt% SGO/SPBI (PA)	0.018 @ 25 °C	–	–	[46]
SGO/PBI/PA	0.052 @ 175 °C	–	–	[54]
PBI-SGO-0.5 (PA)	–	0.024 @ 180 °C	–	[20]
PBI + MSA (PA)	–	0.005 @ 20 °C	–	[33]
sPBI/SIGO-15	–	0.006 @ 120 °C	–	[44]
co-$PNIS_{70/30}$	0.096 @ 25 °C	0.060 @ 25 °C	0.23	[53]
sPSU	0.078 @ 120 °C	0.056 @ 120 °C	0.16	[55]
PBC2.0[THF]	0.124 @ 25 °C	0.024 @ 25 °C	0.67	[56]
M-GOM/oxid	0.018 @ 90 °C	0.002 @ 90 °C	0.80	[57]
PBI/SGO 1:2	0.113 @ 120 °C	0.011 @ 120 °C	0.83	Present work
PBI/SGO 1:3	0.092 @ 120 °C	0.025 @ 120 °C	0.57	Present work

CRediT authorship contribution statement

Matteo Di Virgilio: Writing – original draft, Visualization, Validation, Investigation, Data curation, Conceptualization. **Andrea Basso Peressut:** Writing – review & editing, Validation, Methodology, Formal analysis. **Sophie Provato:** Writing – original draft, Investigation, Formal analysis, Data curation. **Saverio Latorrata:** Writing – review & editing, Supervision, Resources, Methodology, Conceptualization.

Declaration of competing interest

The authors declare that they have no known competing financial interests or personal relationships that could have appeared to influence the work reported in this paper.

Acknowledgements

The authors would like to express deep gratitude to Dr. Eirini Ioannou of the Regional Center of Advanced Technology and Materials (RCPTM), Czech Republic, for the precious help in performing surface and cross-sectional SEM analysis.

References

[1] Department of Economic and Social Affairs (Population Division), World Population Prospects, 2022. www.un.org/development/desa/pd/.
[2] International Energy Agency, World Energy Outlook, 2023. https://www.iea.org/reports/world-energy-outlook-2023.
[3] IPCC, Strengthening and implementing the global response, in: Glob. Warm. 1.5°C, Cambridge University Press, 2018, pp. 313–444, https://doi.org/10.1017/9781009157940.006.
[4] United Nations, Provisional State of the Global Climate 2023, 2023, https://doi.org/10.18356/9789213586891.
[5] Q. Che, Z. Zhu, N. Chen, X. Zhai, Methylimidazolium group – modified polyvinyl chloride (PVC) doped with phosphoric acid for high temperature proton exchange membranes, Mater. Des. 87 (2015) 1047–1055, https://doi.org/10.1016/j.matdes.2015.08.092.
[6] M.V. Nguyen, H.C. Dong, D. Nguyen-Manh, N.H. Vu, T.T. Trinh, T.B. Phan, Effect of hydrogen-bonding networks in water on the proton conductivity properties of metal–organic frameworks, J. Sci. Adv. Mater. Devices. 6 (2021) 509–515, https://doi.org/10.1016/j.jsamd.2021.06.005.
[7] U. Lucia, Overview on fuel cells, Renew. Sustain. Energy Rev. 30 (2014) 164–169, https://doi.org/10.1016/j.rser.2013.09.025.
[8] Y. Wang, D.F. Ruiz Diaz, K.S. Chen, Z. Wang, X.C. Adroher, Materials, technological status, and fundamentals of PEM fuel cells – a review, Mater. Today 32 (2020) 178–203, https://doi.org/10.1016/j.mattod.2019.06.005.
[9] M.M. Tellez-Cruz, J. Escorihuela, O. Solorza-Feria, V. Compañ, Proton exchange membrane fuel cells (PEMFCs): advances and challenges, Polymers 13 (2021) 3064, https://doi.org/10.3390/polym13183064.
[10] S. Ahmad, T. Nawaz, A. Ali, M.F. Orhan, A. Samreen, A.M. Kannan, An overview of proton exchange membranes for fuel cells: materials and manufacturing, Int. J. Hydrogen Energy 47 (2022) 19086–19131, https://doi.org/10.1016/j.ijhydene.2022.04.099.
[11] R. Lohmann, I.T. Cousins, J.C. DeWitt, J. Glüge, G. Goldenman, D. Herzke, A. B. Lindstrom, M.F. Miller, C.A. Ng, S. Patton, M. Scheringer, X. Trier, Z. Wang, Are fluoropolymers really of low concern for human and environmental health and separate from other PFAS? Environ. Sci. Technol. 54 (2020) 12820–12828, https://doi.org/10.1021/acs.est.0c03244.
[12] M. Di Virgilio, A. Basso Peressut, V. Arosio, A. Arrigoni, S. Latorrata, G. Dotelli, Functional and environmental performances of novel electrolytic membranes for pem fuel cells: a lab-scale case study, Cleanroom Technol. 5 (2023) 74–93, https://doi.org/10.3390/cleantechnol5010005.
[13] M.F.A. Kamaroddin, N. Sabli, T.A. Tuan Abdullah, S.I. Siajam, L.C. Abdullah, A. Abdul Jalil, A. Ahmad, Membrane-based electrolysis for hydrogen production: a review, Membranes 11 (2021) 810, https://doi.org/10.3390/membranes11110810.
[14] N. Seselj, D. Aili, S. Celenk, L.N. Cleemann, H.A. Hjuler, J.O. Jensen, K. Azizi, Q. Li, Performance degradation and mitigation of high temperature polybenzimidazole-based polymer electrolyte membrane fuel cells, Chem. Soc. Rev. 52 (2023) 4046–4070, https://doi.org/10.1039/D3CS00072A.
[15] M.A. Haque, A.B. Sulong, K.S. Loh, E.H. Majlan, T. Husaini, R.E. Rosli, Acid doped polybenzimidazoles based membrane electrode assembly for high temperature proton exchange membrane fuel cell: a review, Int. J. Hydrogen Energy 42 (2017) 9156–9179, https://doi.org/10.1016/j.ijhydene.2016.03.086.
[16] L.K. Seng, M.S. Masdar, L.K. Shyuan, Ionic liquid in phosphoric acid-doped polybenzimidazole (PA-PBI) as electrolyte membranes for pem fuel cells: a review, Membranes 11 (2021) 728, https://doi.org/10.3390/membranes11100728.
[17] N. Üregen, K. Pehlivanoğlu, Y. Özdemir, Y. Devrim, Development of polybenzimidazole/graphene oxide composite membranes for high temperature PEM fuel cells, Int. J. Hydrogen Energy 42 (2017) 2636–2647, https://doi.org/10.1016/j.ijhydene.2016.07.009.
[18] S. Archana, K.Y. Kumar, B.K. Jayanna, S. Olivera, A. Anand, M.K. Prashanth, H. B. Muralidhara, Versatile Graphene oxide decorated by star shaped Zinc oxide nanocomposites with superior adsorption capacity and antimicrobial activity, J. Sci. Adv. Mater. Devices. 3 (2018) 167–174, https://doi.org/10.1016/j.jsamd.2018.02.002.
[19] J. Kim, K. Kim, T. Ko, J. Han, J.-C. Lee, Polybenzimidazole composite membranes containing imidazole functionalized graphene oxide showing high proton conductivity and improved physicochemical properties, Int. J. Hydrogen Energy 46 (2021) 12254–12262, https://doi.org/10.1016/j.ijhydene.2020.02.193.
[20] R.R.R. Sulaiman, R. Walvekar, W.Y. Wong, M. Khalid, M.M. Pang, Proton conductivity enhancement at high temperature on polybenzimidazole membrane electrolyte with acid-functionalized graphene oxide fillers, Membranes 12 (2022) 344, https://doi.org/10.3390/membranes12030344.
[21] Z.U. Khan, A. Kausar, H. Ullah, A. Badshah, W.U. Khan, A review of graphene oxide, graphene buckypaper, and polymer/graphene composites: properties and fabrication techniques, J. Plast. Film Sheeting 32 (2016) 336–379, https://doi.org/10.1177/8756087915614612.
[22] D. Dhamodharan, P.P. Ghoderao, V. Dhinakaran, S. Mubarak, N. Divakaran, H.-S. Byun, A review on graphene oxide effect in energy storage devices, J. Ind. Eng. Chem. 106 (2022) 20–36, https://doi.org/10.1016/j.jiec.2021.10.033.
[23] A. Basso Peressut, M. Di Virgilio, A. Bombino, S. Latorrata, E. Muurinen, R. L. Keiski, G. Dotelli, Investigation of sulfonated graphene oxide as the base material for novel proton exchange membranes, Molecules 27 (2022) 1507, https://doi.org/10.3390/molecules27051507.
[24] Y.N. Yusoff, K.S. Loh, W.Y. Wong, W.R.W. Daud, T.K. Lee, Sulfonated graphene oxide as an inorganic filler in promoting the properties of a polybenzimidazole membrane as a high temperature proton exchange membrane, Int. J. Hydrogen Energy 45 (2020) 27510–27526, https://doi.org/10.1016/j.ijhydene.2020.07.026.
[25] Y. Devrim, G.N. Bulanık Durmuş, Composite membrane by incorporating sulfonated graphene oxide in polybenzimidazole for high temperature proton exchange membrane fuel cells, Int. J. Hydrogen Energy 47 (2022) 9004–9017, https://doi.org/10.1016/j.ijhydene.2021.12.257.
[26] K. Maegawa, H. Nagai, R. Kumar, M.M. Abdel-Galeil, W.K. Tan, A. Matsuda, Development of polybenzimidazole modification with open-edges/porous-reduced graphene oxide composite membranes for excellent stability and improved PEM fuel cell performance, Mater. Chem. Phys. 294 (2023) 126994, https://doi.org/10.1016/j.matchemphys.2022.126994.
[27] I.I. Ponomarev, D.Y. Razorenov, K.M. Skupov, I.I. Ponomarev, Y.A. Volkova, K. A. Lyssenko, A.A. Lysova, E.S. Vtyurina, M.I. Buzin, Z.S. Klemenkova, Self-phosphorylated polybenzimidazole: an environmentally friendly and economical approach for hydrogen/air high-temperature polymer-electrolyte membrane fuel cells, Membranes 13 (2023) 552, https://doi.org/10.3390/membranes13060552.
[28] J. Peng, X. Fu, J. Luo, L. Wang, X. Peng, Fabrication of high performance high-temperature proton exchange membranes through constructing stable cation-rich domain in polybenzimidazole membrane, Chem. Eng. J. 453 (2023) 139609, https://doi.org/10.1016/j.cej.2022.139609.
[29] X. Sun, S. Simonsen, T. Norby, A. Chatzitakis, Composite membranes for high temperature pem fuel cells and electrolysers: a critical review, Membranes 9 (2019) 83, https://doi.org/10.3390/membranes9070083.
[30] M. Di Virgilio, A. Basso Peressut, A. Pontoglio, S. Latorrata, G. Dotelli, Study of innovative GO/PBI composites as possible proton conducting membranes for electrochemical devices, Membranes 13 (2023) 428, https://doi.org/10.3390/membranes13040428.
[31] R. Haider, Y. Wen, Z.-F. Ma, D.P. Wilkinson, L. Zhang, X. Yuan, S. Song, J. Zhang, High temperature proton exchange membrane fuel cells: progress in advanced materials and key technologies, Chem. Soc. Rev. 50 (2021) 1138–1187, https://doi.org/10.1039/D0CS00296H.
[32] A. Shirdast, A. Sharif, M. Abdollahi, Effect of the incorporation of sulfonated chitosan/sulfonated graphene oxide on the proton conductivity of chitosan membranes, J. Power Sources 306 (2016) 541–551, https://doi.org/10.1016/j.jpowsour.2015.12.076.
[33] Y. Wang, K. Feng, L. Ding, L. Wang, X. Han, Influence of solvent on ion conductivity of polybenzimidazole proton exchange membranes for vanadium redox flow batteries, Chin. J. Chem. Eng. 28 (2020) 1701–1708, https://doi.org/10.1016/j.cjche.2020.01.009.
[34] A. Singh, P.S. Dhapola, S. Kumar, S. Konwar, P.K. Singh, A.M.M. Ali, D. Agarwal, D. Singh, K. Strzałkowski, M.Z.A. Yahya, S.V. Savilov, B. Joshi, Highly conducting ionic liquid doped polymer electrolyte for energy storage applications, J. Sci. Adv. Mater. Devices. 7 (2022) 100511, https://doi.org/10.1016/j.jsamd.2022.100511.
[35] S. Latorrata, C. Cristiani, A. Basso Peressut, L. Brambilla, M. Bellotto, G. Dotelli, E. Finocchio, P. Gallo Stampino, G. Ramis, Reduced graphene oxide membranes as potential self-assembling filter for wastewater treatment, Minerals 11 (2020) 15, https://doi.org/10.3390/min11010015.
[36] X.-Z. Yuan, C. Song, H. Wang, J. Zhang, Impedance and its corresponding electrochemical processes, in: Electrochem. Impedance Spectrosc. PEM Fuel Cells, Springer London, London, 2010, pp. 95–138, https://doi.org/10.1007/978-1-84882-846-9_3.
[37] X.-Z. Yuan, C. Song, H. Wang, J. Zhang, EIS equivalent circuits, in: Electrochem. Impedance Spectrosc. PEM Fuel Cells, Springer London, London, 2010, pp. 139–192, https://doi.org/10.1007/978-1-84882-846-9_4.
[38] X. Luo, G. Lau, M. Tesfaye, C.R. Arthurs, I. Cordova, C. Wang, M. Yandrasits, A. Kusoglu, Thickness dependence of proton-exchange-membrane properties, J. Electrochem. Soc. 168 (2021) 104517, https://doi.org/10.1149/1945-7111/ac2973.

[39] A. Figoli, T. Marino, S. Simone, E. Di Nicolò, X.-M. Li, T. He, S. Tornaghi, E. Drioli, Towards non-toxic solvents for membrane preparation: a review, Green Chem. 16 (2014) 4034, https://doi.org/10.1039/C4GC00613E.
[40] D. Matveev, V. Vasilevsky, V. Volkov, T. Plisko, A. Shustikov, A. Volkov, A. Bildyukevich, Fabrication of ultrafiltration membranes from non-toxic solvent dimethylsulfoxide: benchmarking of commercially available acrylonitrile co-polymers, J. Environ. Chem. Eng. 10 (2022) 107061, https://doi.org/10.1016/j.jece.2021.107061.
[41] D. Plackett, A. Siu, Q. Li, C. Pan, J.O. Jensen, S.F. Nielsen, A.A. Permyakova, N. J. Bjerrum, High-temperature proton exchange membranes based on polybenzimidazole and clay composites for fuel cells, J. Membr. Sci. 383 (2011) 78–87, https://doi.org/10.1016/j.memsci.2011.08.038.
[42] D. Konios, M.M. Stylianakis, E. Stratakis, E. Kymakis, Dispersion behaviour of graphene oxide and reduced graphene oxide, J. Colloid Interface Sci. 430 (2014) 108–112, https://doi.org/10.1016/j.jcis.2014.05.033.
[43] A. Alanazi, S. Alshehri, M. Altamimi, F. Shakeel, Solubility determination and three dimensional Hansen solubility parameters of gefitinib in different organic solvents: experimental and computational approaches, J. Mol. Liq. 299 (2020) 112211, https://doi.org/10.1016/j.molliq.2019.112211.
[44] M.A. Imran, G. He, X. Wu, X. Yan, T. Li, A.S. Khan, Fabrication and characterization of sulfonated polybenzimidazole/sulfonated imidized graphene oxide hybrid membranes for high temperature proton exchange membrane fuel cells, J. Appl. Polym. Sci. 136 (2019) 1–13, https://doi.org/10.1002/app.47892.
[45] W.W. Ng, H.S. Thiam, Y.L. Pang, Y.S. Lim, J. Wong, L.H. Saw, Self-sustainable, self-healable sulfonated graphene oxide incorporated nafion/poly(vinyl alcohol) proton exchange membrane for direct methanol fuel cell applications, J. Environ. Chem. Eng. 11 (2023) 111151, https://doi.org/10.1016/j.jece.2023.111151.
[46] S. Mondal, F. Papiya, S.N. Ash, P.P. Kundu, Composite membrane of sulfonated polybenzimidazole and sulfonated graphene oxide for potential application in microbial fuel cell, J. Environ. Chem. Eng. 9 (2021) 104945, https://doi.org/10.1016/j.jece.2020.104945.
[47] X. Zhao, B. Nan, Y. Lu, C. Zhao, S. Xu, Phosphorylated graphene oxide-reinforced polybenzimidazole composite membrane for high-temperature proton exchange membrane fuel cell, J. Polym. Res. 28 (2021) 480, https://doi.org/10.1007/s10965-021-02846-x.
[48] S.B. Aziz, M.A. Brza, H.M. Hamsan, M.F.Z. Kadir, R.T. Abdulwahid, Electrochemical characteristics of solid state double-layer capacitor constructed from proton conducting chitosan-based polymer blend electrolytes, Polym. Bull. 78 (2021) 3149–3167, https://doi.org/10.1007/s00289-020-03278-1.
[49] P.A. Christensen, S.W.M. Jones, An in situ FTIR study of undoped PolyBenzoImadazole as a function of relative humidity, Polym. Degrad. Stabil. 105 (2014) 211–217, https://doi.org/10.1016/j.polymdegradstab.2014.04.020.
[50] C.M. Phela, R. Sigwadi, P.F. Msomi, Sulfonated graphene oxide/sulfonated poly (2,6- dimethyl – 1,4-phenylene oxide) as a potential proton exchange membrane for iron air flow battery application, Polym. Adv. Technol. 34 (2023) 2044–2056, https://doi.org/10.1002/pat.6030.
[51] S. Ma, Z. Siroma, H. Tanaka, Anisotropic conductivity over in-plane and thickness directions in nafion-117, J. Electrochem. Soc. 153 (2006) A2274, https://doi.org/10.1149/1.2357727.
[52] T. Soboleva, Z. Xie, Z. Shi, E. Tsang, T. Navessin, S. Holdcroft, Investigation of the through-plane impedance technique for evaluation of anisotropy of proton conducting polymer membranes, J. Electroanal. Chem. 622 (2008) 145–152, https://doi.org/10.1016/j.jelechem.2008.05.017.
[53] U. Zavorotnaya, I. Ponomarev, Y. Volkova, A. Modestov, V. Andreev, A. Privalov, M. Vogel, V. Sinitsyn, Preparation and study of sulfonated Co-polynaphthoyleneimide proton-exchange membrane for a H2/air fuel cell, Materials 13 (2020) 5297, https://doi.org/10.3390/ma13225297.
[54] C. Xu, Y. Cao, R. Kumar, X. Wu, X. Wang, K. Scott, A polybenzimidazole/sulfonated graphite oxide composite membrane for high temperature polymer electrolyte membrane fuel cells, J. Mater. Chem. 21 (2011) 11359, https://doi.org/10.1039/c1jm11159k.
[55] C. Simari, E. Lufrano, G.A. Corrente, I. Nicotera, Anisotropic behavior of mechanically extruded sulfonated polysulfone: implications for proton exchange membrane fuel cell applications, Solid State Ionics 362 (2021) 115581, https://doi.org/10.1016/J.SSI.2021.115581.
[56] W. Zheng, C.H. Liu, M.P. Nieh, C.J. Cornelius, Sulfonated pentablock copolymer membrane morphological anisotropy and its impact on dimensional swelling, proton conductivity, and the transport of protons and water, Macromolecules 55 (2022) 9269–9281, https://doi.org/10.1021/acs.macromol.2c00987.
[57] M.S.K. Chowdury, Y.J. Cho, P.Y. Ji, J.S. Min, S.B. Park, Y. Park, Sulfonic acid (-HSO3) functionalization effect on graphene oxide membrane by (3 mercaptopropyl) trimethoxysilane and their applications in hydrogen membrane fuel cells, Solid State Ionics 404 (2024) 116411, https://doi.org/10.1016/j.ssi.2023.116411.